Supplementary Materials

Laser annealing-induced phase transformation behaviors of multicomponent metal alloy, oxide and nitride nanoparticle combinations

Yun Li[1], Yee Yan Tay[1], Pio J. S. Buenconsejo[1], William Manalastas, Jr. [1], Wei Han Tu[1], Hong Kit Lim[1,2], Teddy Salim[1], Michael O. Thompson[3], Srinivasan Madhavi[1,2], Chor Yong Tay[1,2], Kwan W. Tan[1,*]

Affiliations:

[1]School of Materials Science and Engineering, Nanyang Technological University, Singapore 639798, Singapore.

[2]Energy Research Institute at Nanyang Technological University, Singapore 637553, Singapore.

[3]Department of Materials Science and Engineering, Cornell University, Ithaca, NY 14853, USA.

*Corresponding author. Email: kwtan@ntu.edu.sg

Table S1.
Constants used in the FEA simulation.

Property	**Pt**	**Carbon**	**Al**	**Laser**
R, reflectance	0.633			
α (m^{-1}), absorption coefficient	4.9×10^{7}			
r_x (μm), beam width (FWHM)				50
r_z (μm), beam length (FWHM)				200
P (W), laser power				0.5–2
t_{dwell} (ms), laser annealing dwell				0.25–250
T_0 (K), ambient temperature	293.15	293.15	293.15	
ρ (kg m^{-3}), density	21450	53	2700	
k (W m^{-1} K^{-1}), thermal conductivity	71.6	0.35	237	
C_p (J K^{-1} kg^{-1}), specific heat capacity	133	eq S6	904	
ε, surface emissivity	0.47	1	0.09	

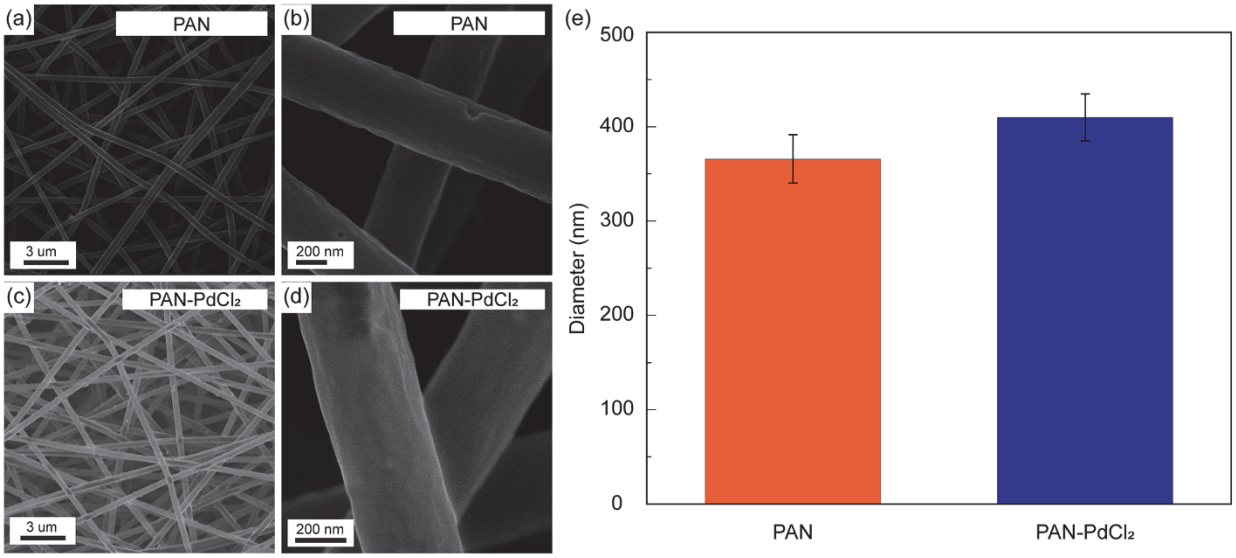

Fig. S1.

(a–d) Representative plan view SEM micrographs of (a, b) uncoated CNF scaffold and (c, d) $PdCl_2$-coated CNF scaffold at (a, c) low and (b, d) high magnifications. (e) The bar chart shows the diameter measurements of individual uncoated and $PdCl_2$-coated CNFs obtained from plan view SEM images. The Pd salt coating thickness was ~40 nm.

Table S2.

Physical properties of precursor metal salts and pure metals.

Sample	Atomic Radius (pm)	Melting Temperature (°C)	Electronegativity (Pauling Scale)	Crystal Structure (300 K)	*d*-spacing (nm)	Standard Reduction Potential (eV)
$HAuCl_4$·		254		Monoclinic		
$PdCl_2$		679		Rhombohedral		
$CuCl_2$		100		Distorted		
$NiCl_2$		1001		Monoclinic		
$FeCl_3$		306		Hexagonal		
$AgNO_3$		212		Orthorhombic		
$CoCl_2$		737		Octahedral		
Au	144	1064	2.4	FCC	d_{111} = 2.355 (PDF 01-071-4073)	1.52 (Au^{3+}/Au)
Pd	137	1555	2.2	FCC	d_{111} = 2.2280 (PDF 04-015-9347)	0.915 (Pd^{2+}/Pd)
Cu	128	1085	1.9	FCC	d_{111} = 2.0880 (PDF 00-004-0836)	0.3419 (Cu^{2+}/Cu)
Ni	125	1455	1.8	FCC	d_{111} = 2.0352 (PDF 01-070-1849)	−0.257 (Ni^{2+}/Ni)
Fe	124	1538	1.8	BCC	d_{110} = 2.0269 (PDF 01-071-3763)	−0.037 (Fe^{3+}/Fe)
Ag	144	962	1.9	FCC	d_{111} = 2.3590 (PDF 00-004-0783)	0.7996 (Ag^{+}/Ag)
Co	125	1495	1.8	HCP	d_{111} = 2.0604 (PDF 01-071-4238)	−0.277 (Co^{2+}/Co)

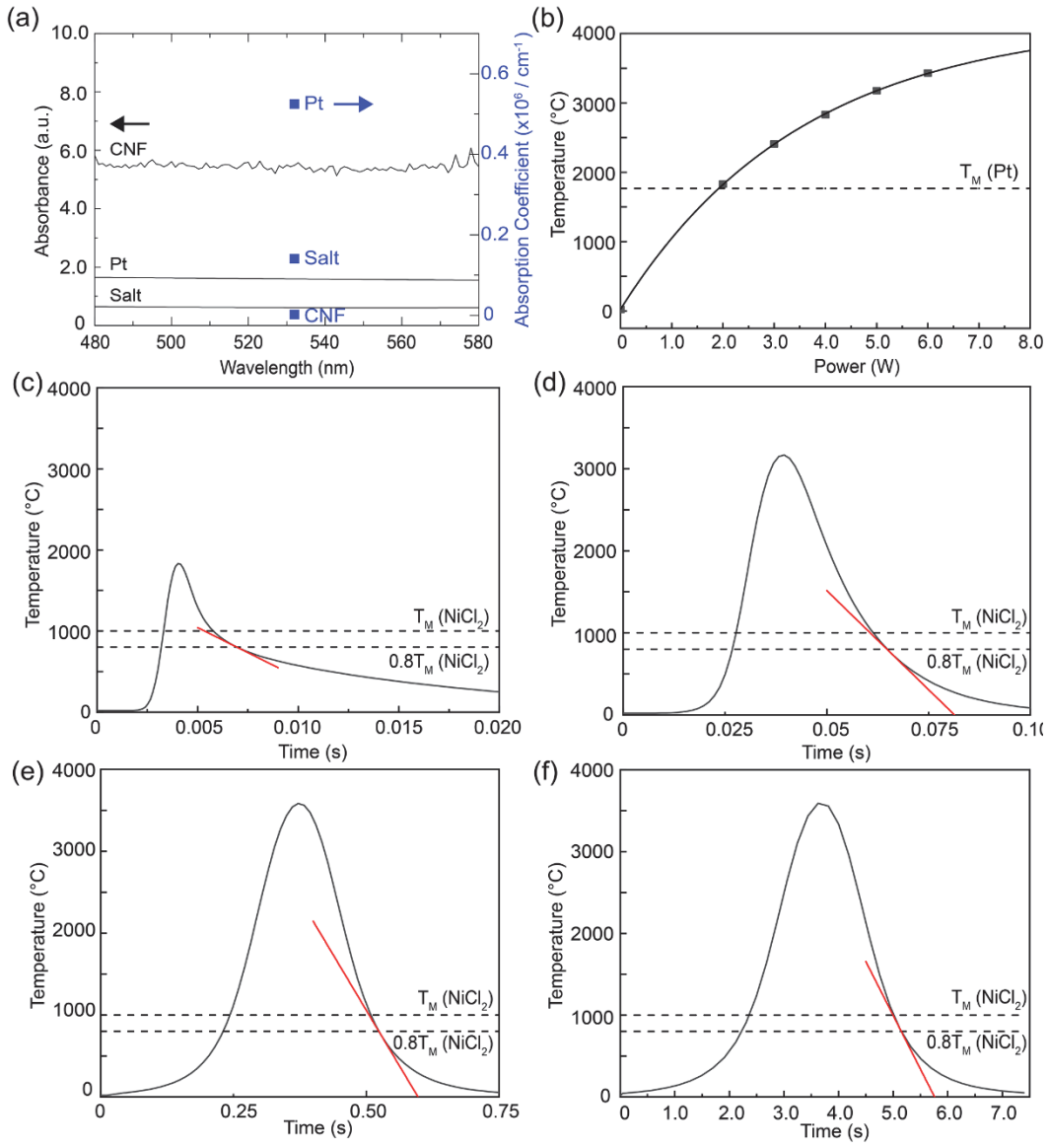

Fig. S2.

(a) UV-vis absorption profiles (black arrow to the left axis) and corresponding adsorption coefficient values (blue arrow to the right axis) of (i) ~60–70 nm thick Pt film, (ii) ~50 µm thick CNF substrate and (iii) ~100–120 nm thick AuPdFeCuNi precursor salt film on glass. Absorption coefficient calculations at 532 nm indicate the metal salt precursors absorb green visible light more strongly than the CNF substrate. We note that the Pt represents the upper limit of the simulated laser temperatures of metal salts. (b) Plot of simulated peak temperature versus laser power of Pt/carbon sample after a single laser irradiation at various powers for 0.25 ms dwell. (c–f) Simulated temperature profiles of Pt/carbon sample after laser irradiation at 2 W for (c) 0.25, (d) 2.5, (e) 25 and (f) 250 ms, respectively. Cooling rates were obtained from the gradients of red-colored tangent lines at ~0.8 time of the melting point of $NiCl_2 \cdot 3H_2O$ (1001 °C). $NiCl_2 \cdot 3H_2O$ was chosen as the reference salt as it has the highest melting point among all the precursors.

Table S3.
Simulated laser annealing characteristics of MC inorganic NPs.

Power (W)	Dwell Time (ms)	T_{peak} (°C)	Melt Duration (ms)	Cooling Rate (K/s)
0.6	2.5	1445	14	5.5×10^4
2	0.25	1830	2.5	1.2×10^5
2	2.5	3165	33	4.8×10^4
2	25	3580	270	1.1×10^4
2	250	3590	2700	1.3×10^3
3	0.25	2410	4.6	7.6×10^4
4	0.25	2830	6.8	5.4×10^4
6	0.25	3430	11	6.0×10^4

Table S4.

Nominal compositional distributions of laser-annealed AuPdFeCuNi MCM NPs obtained from EDS measurements.

Laser Power (W)	Heating Dwell (ms)	Atomic Fraction				
		Au	Pd	Cu	Ni	Fe
2	0.25	0.469	0.351	0.112	0.025	0.043
2	2.5	0.321	0.356	0.047	0.107	0.169
2	25	0.440	0.123	0.237	0.074	0.126
2	250	0.363	0.266	0.108	0.094	0.169
0.6	2.5	0.638	0.250	0.044	0.011	0.057

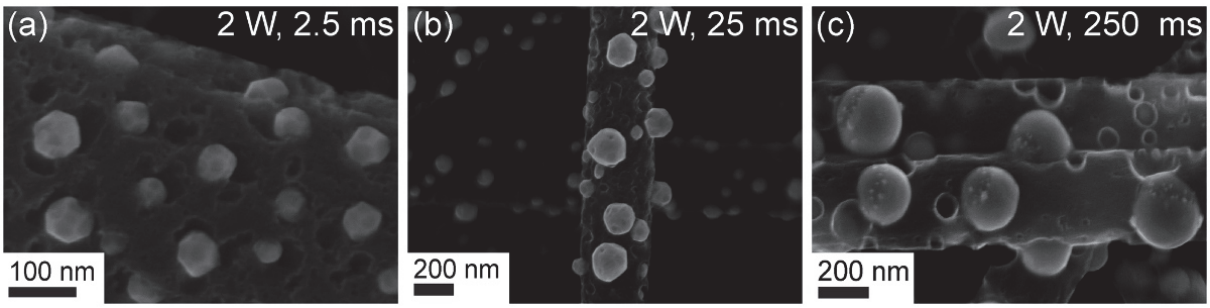

Fig. S3.

Lower magnification SEM images showing the size distributions and area densities of AuPdCuFeNi MCM NPs after laser annealing at 2 W for dwells of (a) 2.5 ms, (b) 25 ms and (c) 250 ms. The MCM NPs typically grew larger but with decreasing size uniformity for longer annealing dwells.

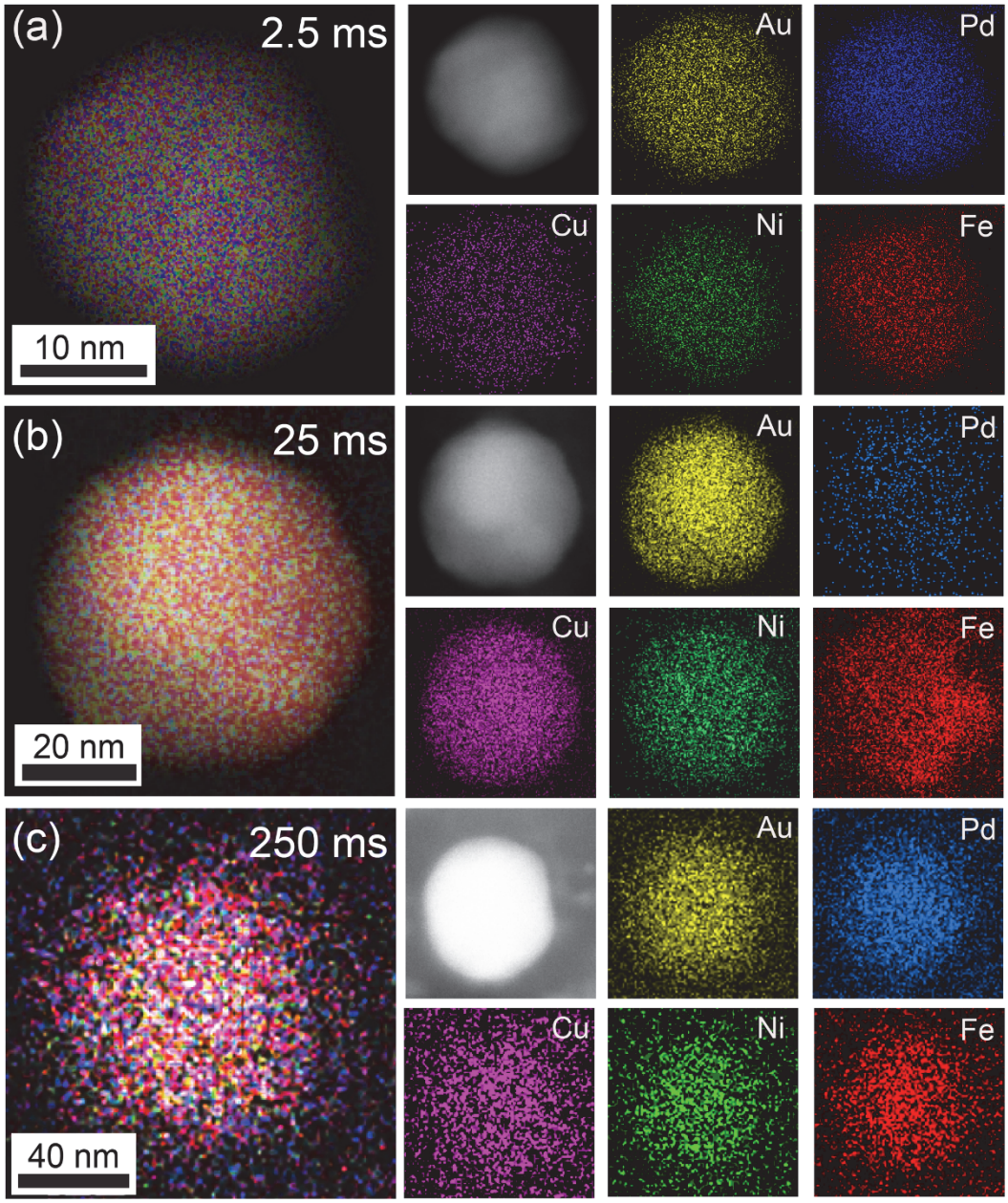

Fig. S4.
HAADF-STEM and EDS elemental mapping analysis of laser-annealed AuPdFeCuNi MCM NPs after laser irradiation at 2 W for dwells of (a) 2.5 ms, (b) 25 ms and (c) 250 ms.

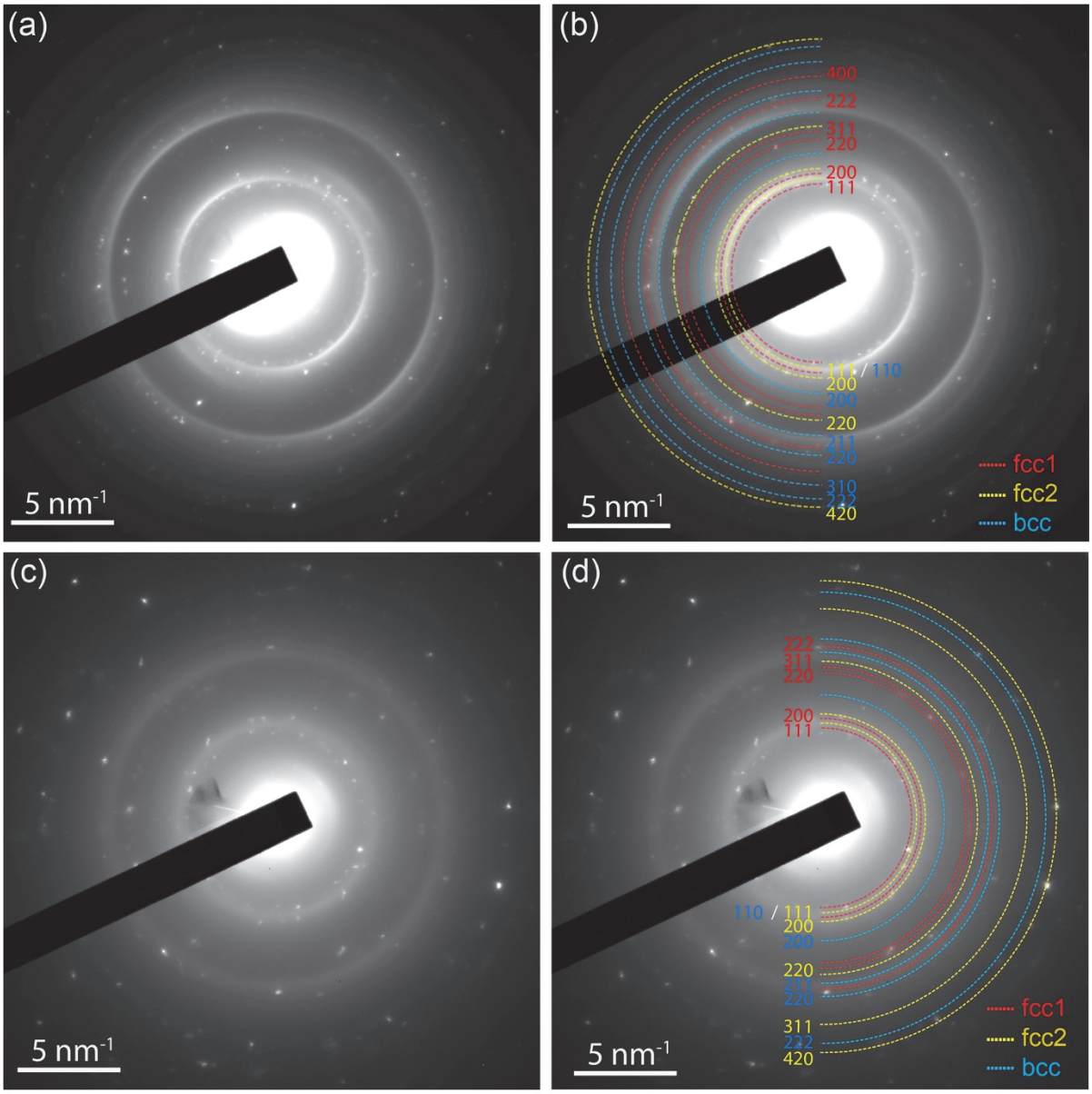

Fig. S5.

Additional selected area electron diffraction patterns of laser-annealed AuPdFeCuNi MCM NPs generated by laser irradiation at 2 W for 2.5 ms, exhibiting the fcc1, fcc2 and bcc phases. The semicircles drawn in panels b and d show the expected *hkl* planes of fcc1, bcc and fcc2 phases present in the neat SAED patterns shown in panels a and c, respectively.

Table S5.

SAED analysis of laser-induced AuPdFeCuNi MCM NPs after irradiation at 2 W for 2.5 ms.

Phase	Plane	Expected Angular Positions (1/*d*, nm^{-1})	Measured Angular Positions (1/d, nm^{-1})		
			Pattern No. 1	Pattern No. 2	Pattern No. 3
fcc1	111	4.24	4.28	4.29	4.38
	200	4.9	4.83	4.84	4.83
	220	6.93	6.97	6.95	7.06
	311	8.13			
	222	8.49	8.4	8.48	8.51
	400	9.8		9.79	
bcc	110	4.51	4.59	4.61	4.64
	200	6.38	6.06	6.51	6.17
	211	7.82	7.85	7.82	
	220	9.03	8.8	8.87	8.91
	310	10.09	10.08	10.15	
	222	11.06	11.02	11.16	11.06
fcc2	111	4.51	4.59	4.61	4.64
	200	5.21	5.06	5.21	5.21
	220	7.37	7.41	7.23	
	311	8.64			
	222	9.03			
	400	10.42	10.37		10.43
	311	11.36	11.44	11.36	

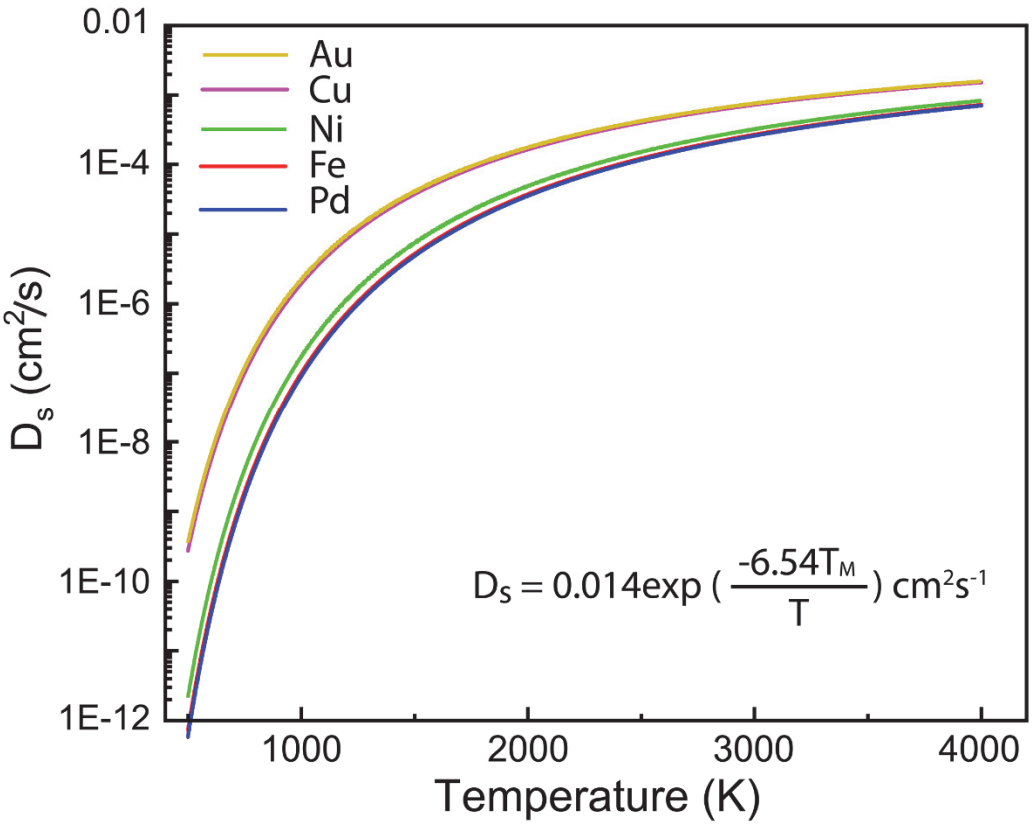

Fig. S6.

Empirical surface diffusivity D_s plots of Au, Cu, Ni, Fe and Pd metals. T_m refers to the melting points of the respective metals.

Table S6.

Surface diffusivity D_S values of pure metals at the peak laser annealing temperatures for various dwells obtained from Fig. S6.

Annealing Dwell (ms)	T_{peak} (°C)	Surface Diffusivity, D_S (cm^2/s)				
		Au	**Pd**	**Cu**	**Ni**	**Fe**
0.25	1830	2.2×10^{-4}	4.8×10^{-5}	2.1×10^{-4}	6.5×10^{-5}	5.0×10^{-5}
2.5	3165	1.1×10^{-3}	4.3×10^{-4}	1.1×10^{-3}	5.2×10^{-4}	4.5×10^{-4}
25	3580	1.5×10^{-3}	6.3×10^{-4}	1.4×10^{-3}	7.5×10^{-4}	6.5×10^{-4}
250	3590	1.5×10^{-3}	6.3×10^{-4}	1.4×10^{-3}	7.5×10^{-4}	6.5×10^{-4}

Table S7.

Characteristic diffusion distance $\sqrt{D_s\tau}$ values of pure metals at the peak laser annealing temperatures for various dwells.

Annealing Dwell (τ, ms)	T_{peak} **(°C)**	**Diffusion Distance,** $\sqrt{D_s\tau}$ **(m)**				
		Au	**Pd**	**Cu**	**Ni**	**Fe**
0.25	1830	2.3×10^{-6}	1.1×10^{-6}	2.3×10^{-6}	1.3×10^{-6}	1.1×10^{-6}
2.5	3165	1.7×10^{-5}	1.0×10^{-5}	1.7×10^{-5}	1.1×10^{-5}	1.1×10^{-5}
25	3580	6.1×10^{-5}	4.0×10^{-5}	5.9×10^{-5}	4.3×10^{-5}	4.0×10^{-5}
250	3590	1.9×10^{-4}	1.3×10^{-4}	1.9×10^{-4}	1.4×10^{-4}	1.3×10^{-4}

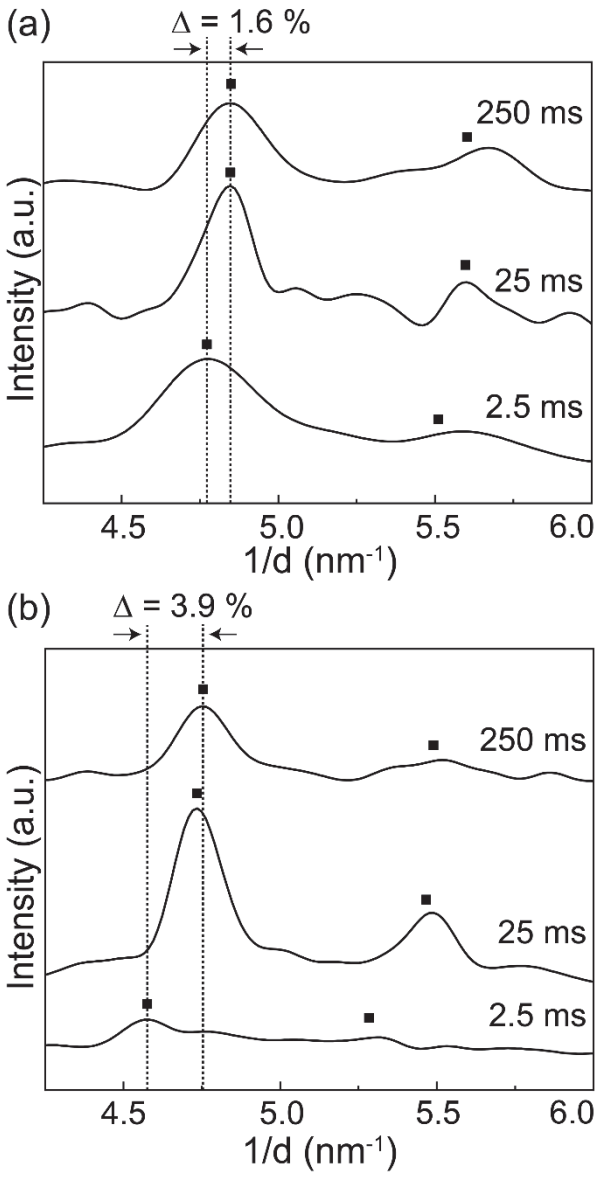

Fig. S7.

WAXS spectra of laser-induced (a) CrFeCoNiMn (Cantor) and (b) CrFeCoNiPd (non-Cantor) systems after laser irradiation at 2 W for various dwells as indicated. For the non-Cantor combination, the shoulder that appeared on the right-hand-side of the primary peak in the WAXS pattern of 2.5 ms dwell in (b) suggests a secondary crystalline phase. This is further supported by a larger red shift of the primary peaks for non-Cantor combination (~3.9%) in (b) compared to Cantor combination (~1.6%) in (a), for longer annealing dwells.

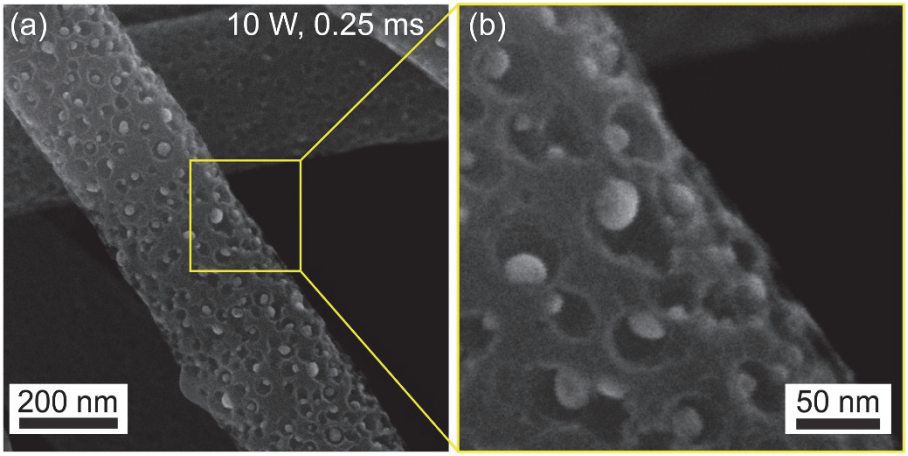

Fig. S8.

SEM images of mono-Pd NPs on CNF scaffold after laser annealing at 10 W for 0.25 ms in ambient air. The resultant Pd NPs likely acted as local hot spots after laser irradiation, inducing localized oxidation and pothole formation on the CNF surface.

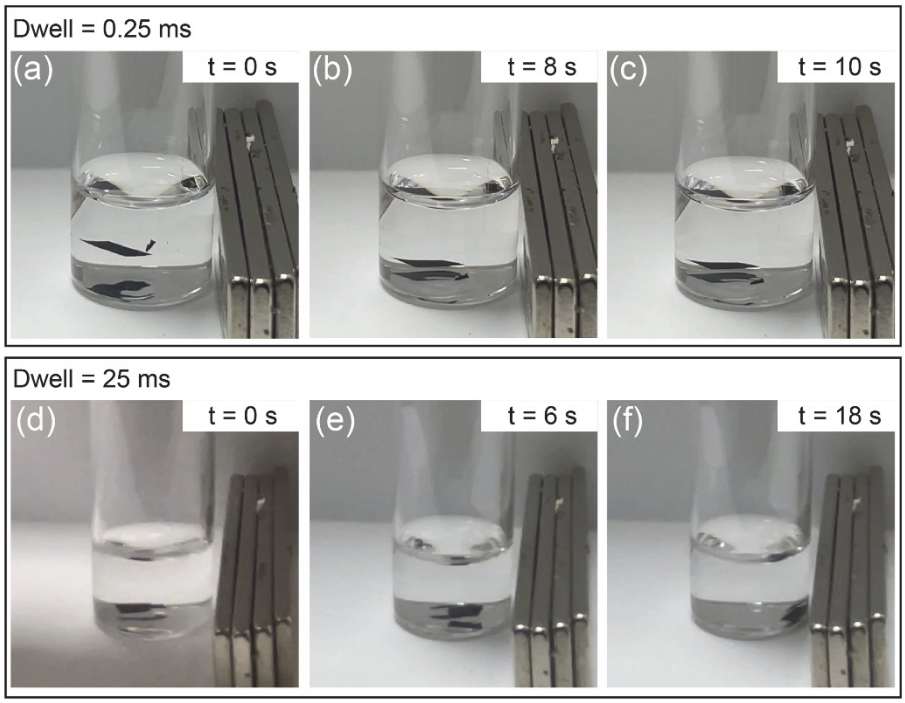

Fig. S9.

Magnetic property tests of laser-annealed AuPdCuFeNi MCM NPs irradiated at 2 W for dwells of (a–c) 0.25 ms and (d–f) 25 ms. (a–c) The 0.25 ms dwell laser-annealed MCM NP/CNF substrate did not move toward the magnet even after 10 seconds. (d–f) Whereas, both pieces of 25 ms dwell MCM NP/CNF substrates gradually moved toward the magnet, confirming the resultant MCM NPs became magnetic due to the increased amounts of ferromagnetic Fe and Ni constituents.

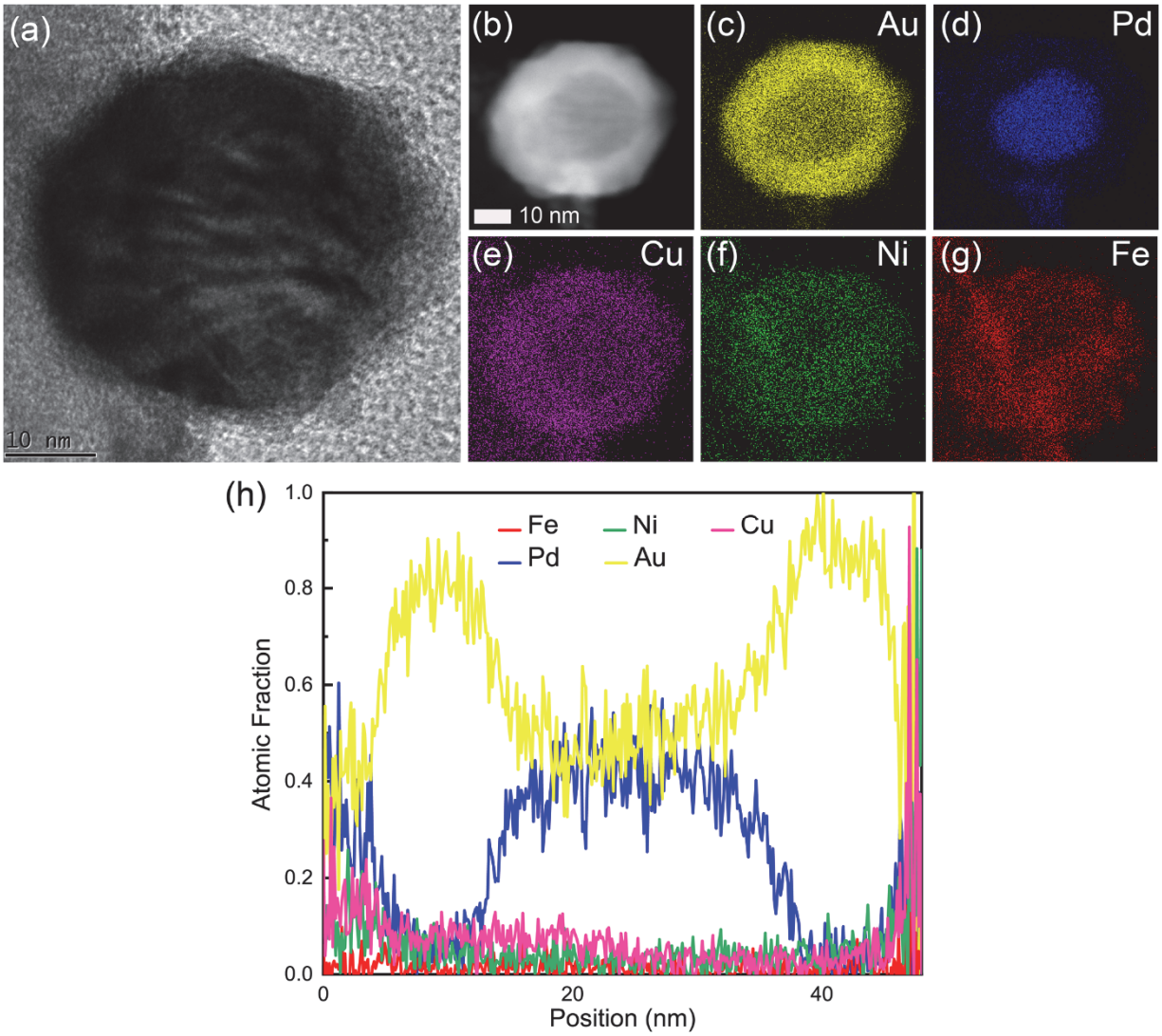

Fig. S10.

(a) TEM, (b) HAADF-STEM, (c–g) EDS elemental mapping analysis and (h) EDS atomic fraction line profiles of a quinary AuPdFeCuNi NP after laser annealing at 0.6 W for 2.5 ms. EDS analysis indicated a Pd-core/Au-rich-shell heterostructured MCM NP.

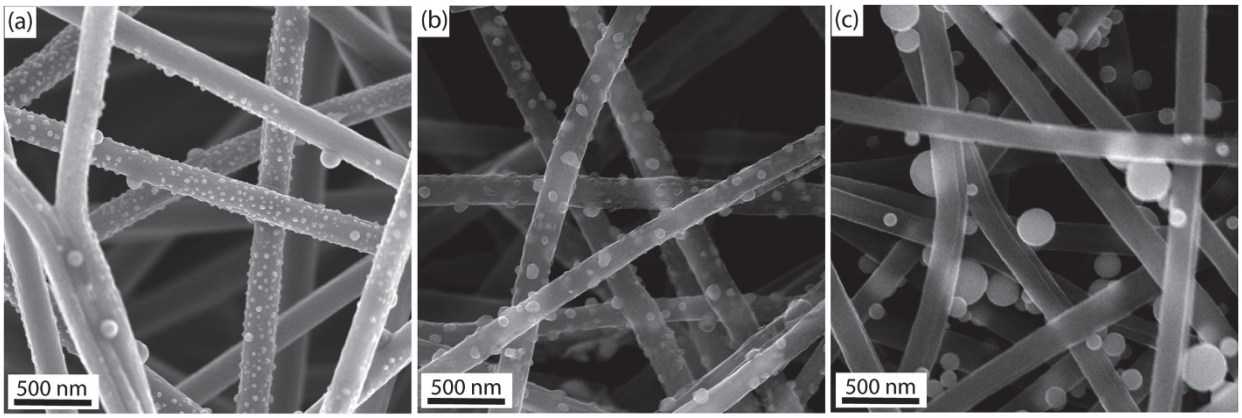

Fig. S11.

SEM of MC ceramic nanoparticles on CNF scaffold after laser annealing at (a) 2 W, (b) 6 W and (c) 12 W, all for 0.25 ms.

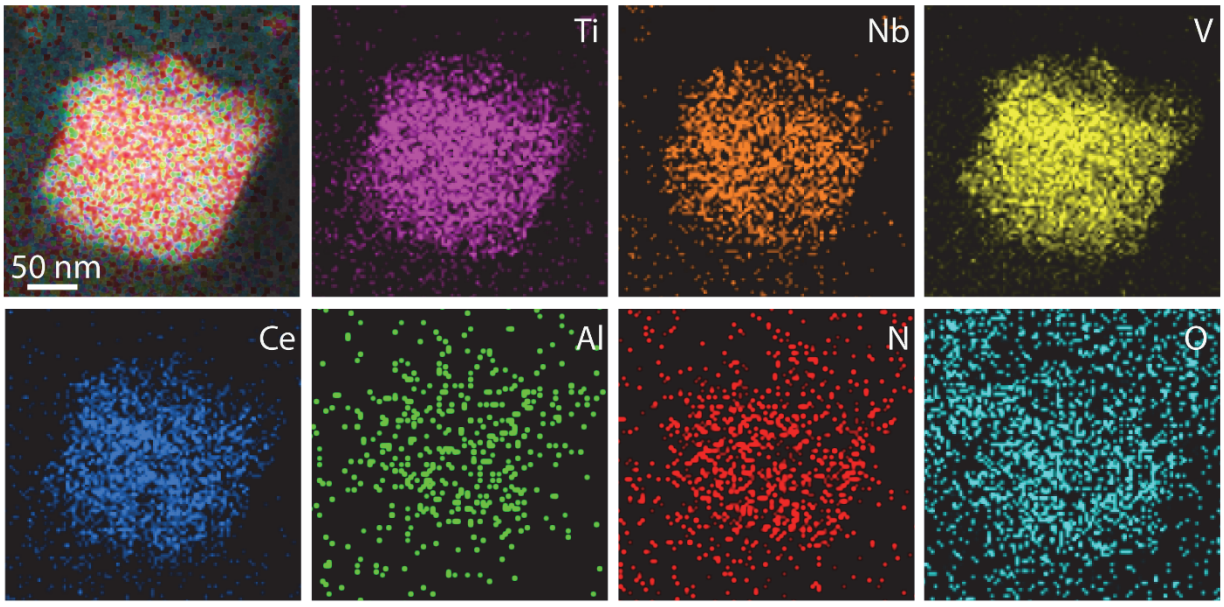

Fig. S12.

HAADF-STEM EDS elemental mapping analysis of a laser-annealed TiNbAlCeV-based NP after irradiation at 12 W for 0.25 ms dwell.

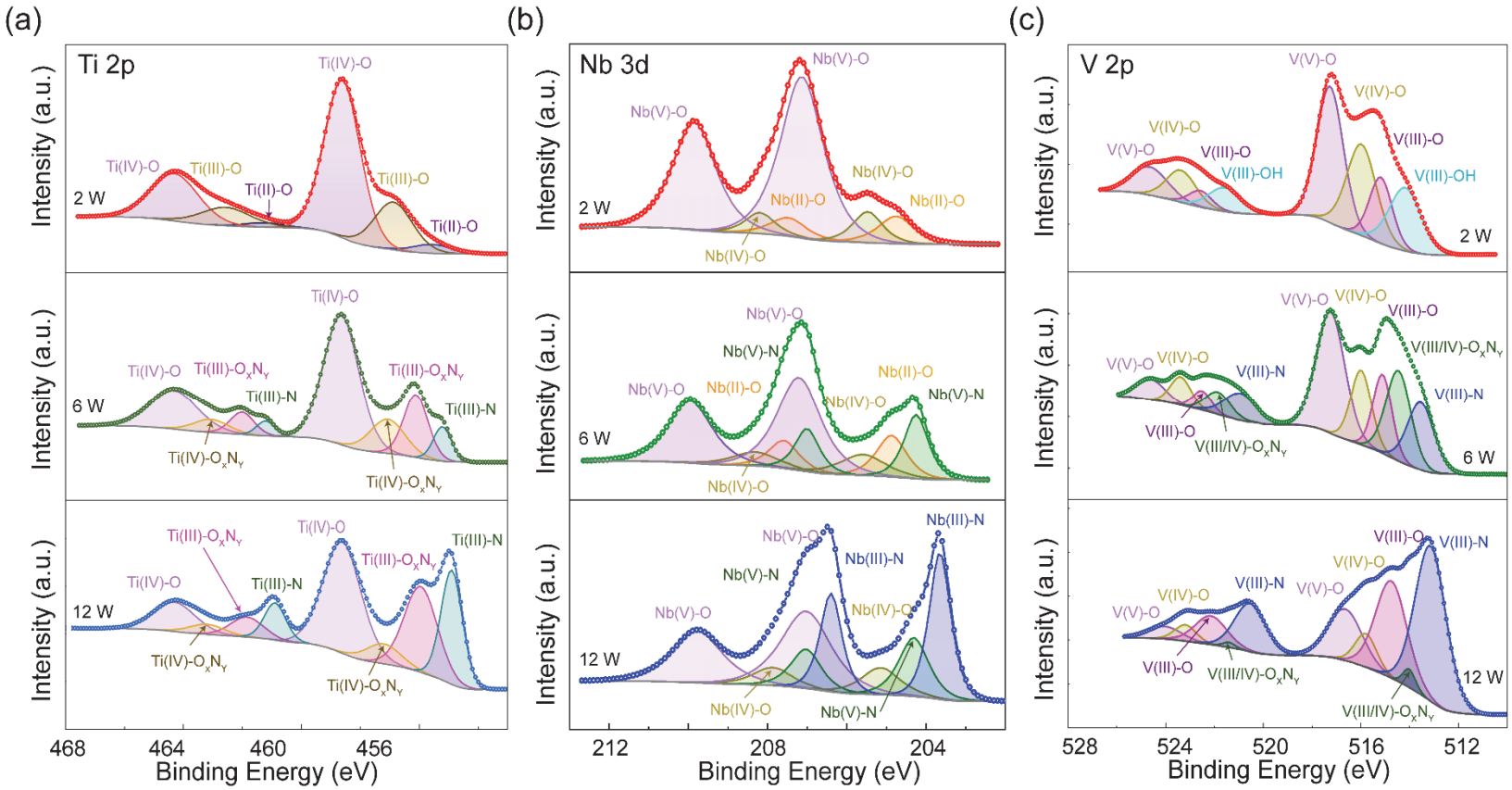

Fig. S13.

High-resolution XPS spectra of TiNbAlCeV-based samples after laser irradiation at 2, 6 and 12 W, respectively, all for 0.25 ms, depicting the resolved component peaks in the (a) Ti 2*p*, (b) Nb 3*d*, (c) V 2*p* regions.

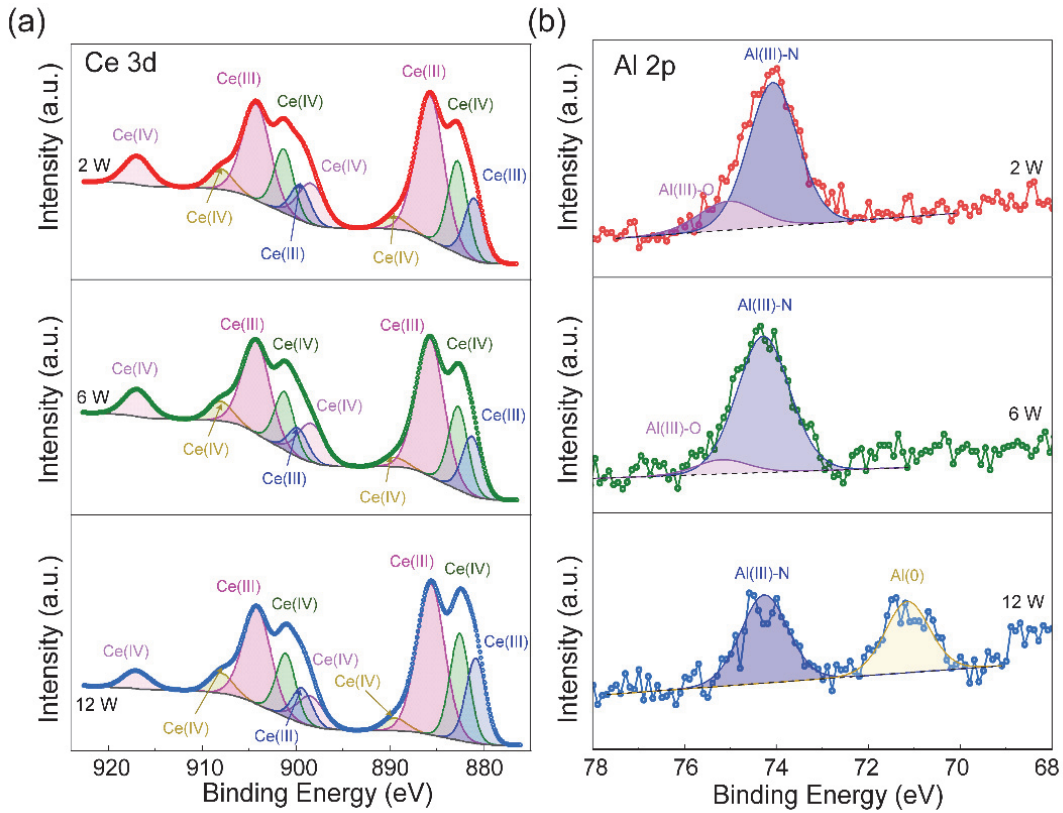

Fig. S14.

High-resolution XPS spectra of TiNbAlCeV-based samples after laser irradiation at 2, 6 and 12 W, respectively, all for 0.25 ms, depicting the resolved component peaks in the (a) Ce 3*d* and (b) Al 2*p* regions.

Table S8.

Binding energy (BE) values of respective component peaks and atomic concentrations in the TiNbAlCeV-based samples after laser irradiation at 2, 6 and 12 W, respectively, all for 0.25 ms.

Sample	State	BE (eV)	Assignment	at.%	State	BE (eV)	Assignment	at.%
2 W	Ti $2p_{3/2}$	458.61	Ti(IV)−O	70.88	Nb $3d_{5/2}$	207.13	Nb(V)−O	78.53
		456.87	Ti(III)−O	24.51		205.47	Nb(IV)−O	10.39
		455.56	Ti(II)−O	4.61		204.76	Nb(II)−O	11.09
	V $2p_{3/2}$	517.26	V(V)−O	35.68	Ce $3d_{5/2}$	882.78	Ce(IV)	39.86
		515.98	V(IV)−O	28.22		881.01	Ce(III)	60.14
		515.18	V(III)−O	14.48				
		514.18	V(III)−OH	21.62	Al $2p$	75.06	Al(III)−O	19.30
						74.08	Al(III)−N	80.70
6 W	Ti $2p_{3/2}$	458.64	Ti(IV)−O	58.42	Nb $3d_{5/2}$	207.21	Nb(V)−O	52.05
		457.07	Ti(IV)−O_xN_y	14.78		205.59	Nb(IV)−O	12.01
		456.11	Ti(III)−O_xN_y	18.73		204.87	Nb(II)−O	15.96
		455.22	Ti(III)−N	8.06		204.25	Nb(V)−N	19.97
	V $2p_{3/2}$	517.24	V(V)−O	30.13	Ce $3d_{5/2}$	882.72	Ce(IV)	39.11
		515.99	V(IV)−O	15.73		881.25	Ce(III)	60.89
		515.11	V(III)−O	13.65				
		514.46	V(III)−O_xN_y	20.71	Al $2p$	75.19	Al(III)−O	9.53
		513.55	V(III)−N	19.78		74.29	Al(III)−N	90.47
12 W	Ti $2p_{3/2}$	458.62	Ti(IV)−O	41.14	Nb $3d_{5/2}$	207.02	Nb(V)−O	39.33
		457.21	Ti(IV)−O_xN_y	7.85		205.12	Nb(IV)−O	10.51
		455.95	Ti(III)−O_xN_y	26.50		204.31	Nb(V)−N	17.95
		454.90	Ti(III)−N	24.50		203.65	Nb(III)−N	32.22
	V $2p_{3/2}$	516.64	V(V)−O	15.70	Ce $3d_{5/2}$	882.57	Ce(IV)	36.86
		515.79	V(IV)−O	7.79		880.85	Ce(III)	63.14
		514.75	V(III)−O	28.65				
		514.01	V(III)−O_xN_y	2.12	Al $2p$	74.27	Al(III)−N	56.95
		513.14	V(III)−N	45.74		71.15	Al(0)	43.05

Table S9.

XPS chemical analysis of ratios of metallic components in TiNbAlCeV-based samples after laser irradiation at 2, 6 and 12 W, respectively, all for 0.25 ms.

Sample	Concentration of Constituent Metals (at %)				
	Ti	Nb	Al	V	Ce
2 W	19.44	30.38	17.03	19.36	13.80
6 W	19.34	23.49	18.59	21.02	17.57
12 W	21.03	32.54	11.24	21.27	13.92

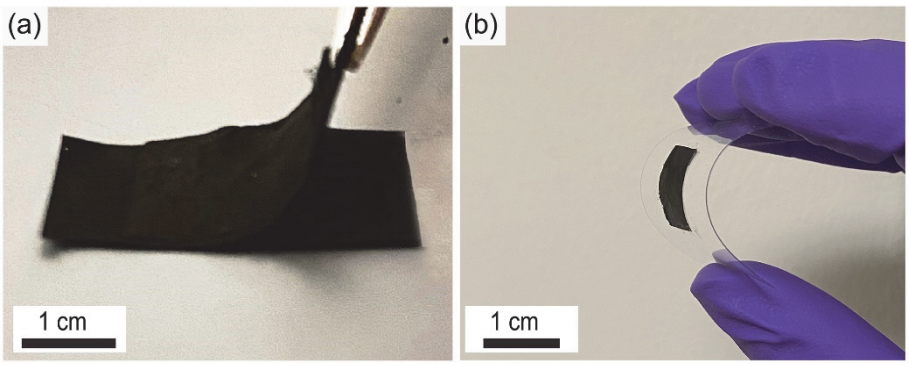

Fig. S15.

Optical images of (a) tape-assisted removal of laser-induced MCM NP-coated CNF substrate and (b) transfer onto a flexible poly(ethylene terephthalate) (PET) substrate.

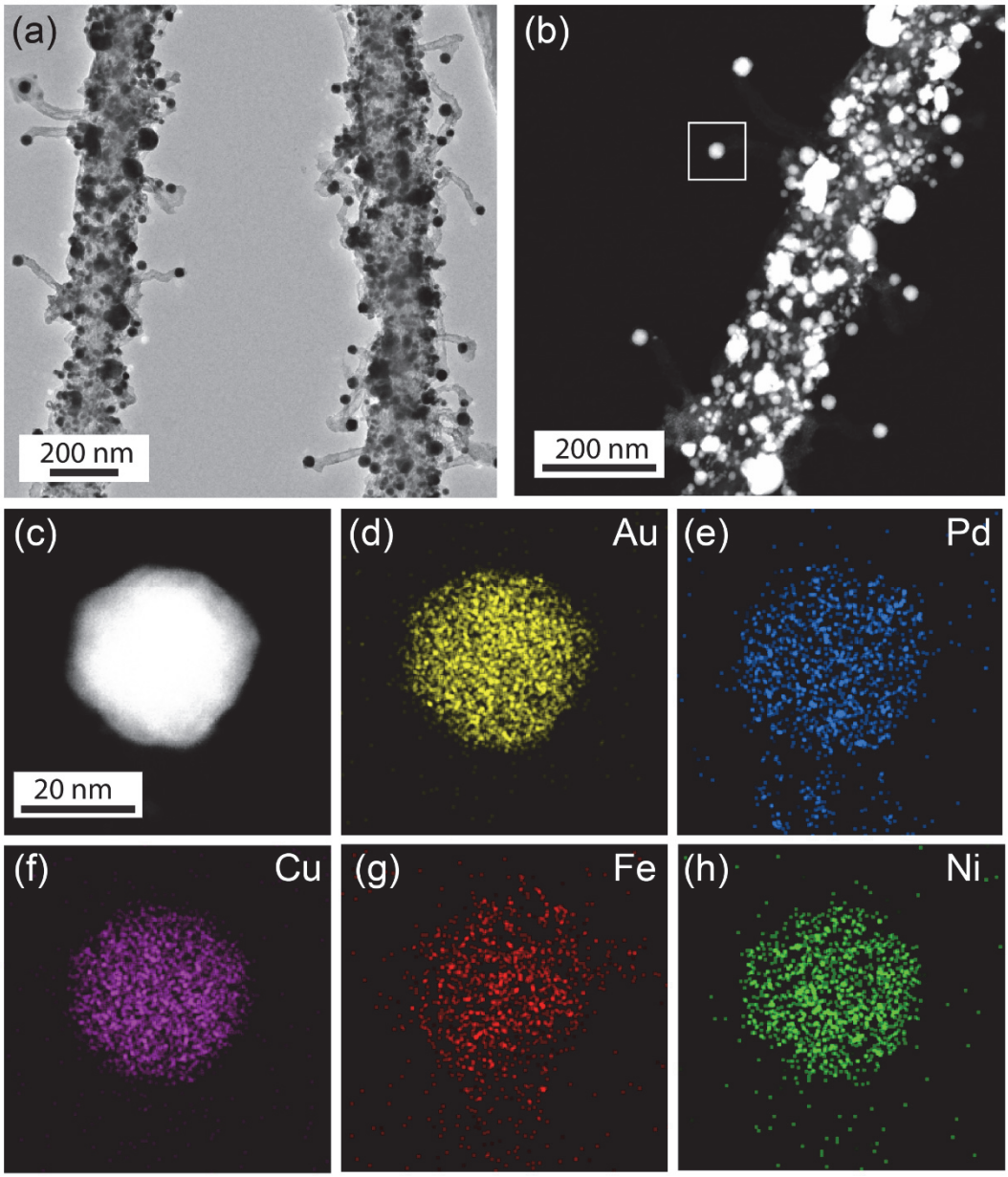

Fig. S16.

(a) Bright-field TEM and (b) HAADF-STEM micrographs of AuPdCuFeNi NP-catalyzed growth of carbon nanotubes after laser annealing at 10 W for 1 ms. (c) HAADF-STEM and (d–h) and elemental EDS images of a representative AuPdCuFeNi NP located at the end of the carbon nanotube denoted by the white box in (b).

Movie S1.

Real-time observations of laser-annealed AuPdCuFeNi NP-coated CNF substrates generated by irradiation at 2 W for 0.25 and 25 ms, respectively, suspended in ethanol and placed next to a magnet. The 25-ms-dwell MCM NP-coated CNF substrates became magnetic after laser irradiation and were attracted toward the magnet.